

ARTICLE

Open Access

RANK promotes colorectal cancer migration and invasion by activating the Ca^{2+} -calcineurin/NFATC1-ACP5 axis

Qian Liang¹, Yun Wang¹, Yingsi Lu¹, Qingqing Zhu¹, Wenlin Xie², Nannan Tang³, Lifen Huang³, Tailai An⁴, Di Zhang¹, Anqi Yan⁵, Shaoyu Liu⁶, Liping Ye¹ and Chengming Zhu¹

Abstract

The tumor necrosis factor (TNF) receptor superfamily member 11a (TNFRSF11a, also known as RANK) was demonstrated to play an important role in tumor metastasis. However, the specific function of RANK in colorectal cancer (CRC) metastasis and the underlying mechanism are unknown. In this study, we found that RANK expression was markedly upregulated in CRC tissues compared with that in matched noncancerous tissues. Increased RANK expression correlated positively with metastasis, higher TNM stage, and worse prognosis in patients with CRC. Overexpression of *RANK* promoted CRC cell metastasis in vitro and in vivo, while knockdown of *RANK* decreased cell migration and invasion. Mechanistically, *RANK* overexpression significantly upregulated the expression of tartrate-resistant acid phosphatase 5 (*TRAP/ACP5*) in CRC cells. Silencing of *ACP5* in *RANK*-overexpressing CRC cells attenuated RANK-induced migration and invasion, whereas overexpression of *ACP5* increased the migration and invasion of *RANK*-silencing cells. The *ACP5* expression was transcriptionally regulated by calcineurin/nuclear factor of activated T cells c1 (NFATC1) axis. The inhibition of calcineurin/NFATC1 significantly decreased *ACP5* expression, and attenuated RANK-induced cell migration and invasion. Furthermore, RANK induced phospholipase C-gamma (PLC γ)-mediated inositol-1,4,5-trisphosphate receptor (IP3R) axis and stromal interaction molecule 1 (STIM1) to evoke calcium (Ca^{2+}) oscillation. The RANK-mediated intracellular Ca^{2+} mobilization stimulated calcineurin to dephosphorylate NFATC1 and induce NFATC1 nuclear translocation. Both blockage of PLC γ -IP3R axis and STIM1 rescued RANK-induced NFATC1 nuclear translocation, *ACP5* expression, and cell metastasis. Our study revealed the functional expression of RANK in human CRC cells and demonstrated that RANK induced the Ca^{2+} -calcineurin/NFATC1-ACP5 axis in the regulation of CRC metastasis, that might be amenable to therapeutic targeting.

Introduction

The tumor necrosis factor (TNF) receptor superfamily member 11a (TNFRSF11a, also known as RANK) and its ligand TNF superfamily member 11 (also known as

RANKL) were first identified as pivotal regulators of osteoclast development in the late 1990s (ref. ¹). Membrane-bound or soluble RANKL from osteoblasts interacts with RANK-expressing pre-osteoclasts to induce osteoclast differentiation for bone remodeling². Over the past two decades the RANKL/RANK axis has been identified as a critical signaling pathway involved in several mechanisms beyond bone homeostasis, most notably in cancer cell migration and bone development³. Abundant RANKL in the bone environment was identified early as a chemoattractant for bone-specific metastasis of epithelial tumors and melanoma that expressed RANK⁴. Luo et al.⁵

Correspondence: Liping Ye (yelp5@mail.sysu.edu.cn) or Chengming Zhu (zhuchm3@mail.sysu.edu.cn)

¹Scientific Research Center, The Seventh Affiliated Hospital, Sun Yat-sen University, Shenzhen, China

²Department of Pathology, The Seventh Affiliated Hospital, Sun Yat-sen University, Shenzhen, China

Full list of author information is available at the end of the article

These authors contributed equally: Qian Liang, Yun Wang

Edited by S. Tait

© The Author(s) 2021



Open Access This article is licensed under a Creative Commons Attribution 4.0 International License, which permits use, sharing, adaptation, distribution and reproduction in any medium or format, as long as you give appropriate credit to the original author(s) and the source, provide a link to the Creative Commons license, and indicate if changes were made. The images or other third party material in this article are included in the article's Creative Commons license, unless indicated otherwise in a credit line to the material. If material is not included in the article's Creative Commons license and your intended use is not permitted by statutory regulation or exceeds the permitted use, you will need to obtain permission directly from the copyright holder. To view a copy of this license, visit <http://creativecommons.org/licenses/by/4.0/>.

proposed that RANKL from tumor-infiltrating inflammatory cells activated RANK on prostate cancer and led to nuclear inhibitor of nuclear factor kappa-B (NF- κ B) kinase subunit alpha (IKK α) activation to control cancer metastasis. Later their group found that tumor-infiltrating CD4⁺CD25⁺FOXP3⁺ T cells were a major source of RANKL production in breast cancer and stimulated breast cancer metastasis through RANKL–RANK signaling⁶. Furthermore, RANK is also involved in the pathogenesis of other solid tumors and nonsolid cancers⁷. Indeed, 89% of carcinomas assessed were RANK immunostaining positive and ~60% of cases exhibited >50% of RANK-positive cancer cells^{8,9}. Studies have proven that increased RANK expression in tumors correlates with worse clinical parameters and progression⁸. The mechanisms by which RANK participates in the cancer development include bone environment-dependent effects and direct RANK signaling. Based on Stephen Paget's seed and soil theory¹⁰, on the one hand, RANKL expressed by osteoblasts and stromal cells in bone is an important chemoattractant for tumor bone metastasis. On the other hand, tumor-associated factors secreted from cancer cells enhance bone resorption by RANKL–RANK-mediated osteoclast activation, which in turn releases tumor growth factors stored in the bone matrix to promote tumor progression¹¹. This bone environment-dependent concept had been demonstrated in primary bone tumors and metastasized bone tumors¹². In addition, many studies have indicated that direct RANK signaling has complex effects on malignancies¹². Activation of RANK can recruit TNF receptor-associated factors to transduce canonical downstream signaling, include NF- κ B, phosphatidylinositol-4,5-bisphosphate 3-kinase, mitogen-activated kinase, and C-Jun N-terminal kinase⁸. The RANK-mediated signaling network is also associated with epithelial to mesenchymal transition, stemness, and metastatic genes^{8,13}.

Santini et al.⁹ found that 75% of colorectal cancer (CRC) tissues were RANK-positive when detected using immunostaining. Studies had shown that RANKL–RANK-mediated bone resorption supported CRC dissemination in bone¹⁴, and blockage of RANKL–RANK signaling could inhibit CRC growth and the bone resorption caused by CRC in vivo^{15,16}. However, the intrinsic role of RANK expressed on CRC remains unclear. In the current study, we identified that RANK expression was upregulated in CRC tissues and correlated with worse prognosis. Functional analyses demonstrated that RANK promoted the metastases of CRC cells both in vitro and in vivo. Mechanistically, RANK overexpression in CRC not only activated the canonical key downstream of RANK signaling, but also notably induced the Ca²⁺ oscillation dependent of phospholipase C-gamma (PLC γ)-mediated inositol-1,4,5-trisphosphate (IP3) receptor (IP3R) axis and stromal interaction molecule 1 (STIM1) to activate

calcineurin/nuclear factor of activated T-cells c1 (NFATC1)-tartrate-resistant acid phosphatase 5 (TRAP/ACP5) axis to promote metastasis. Our results highlighted the intrinsic role and mechanism of RANK in CRC metastasis.

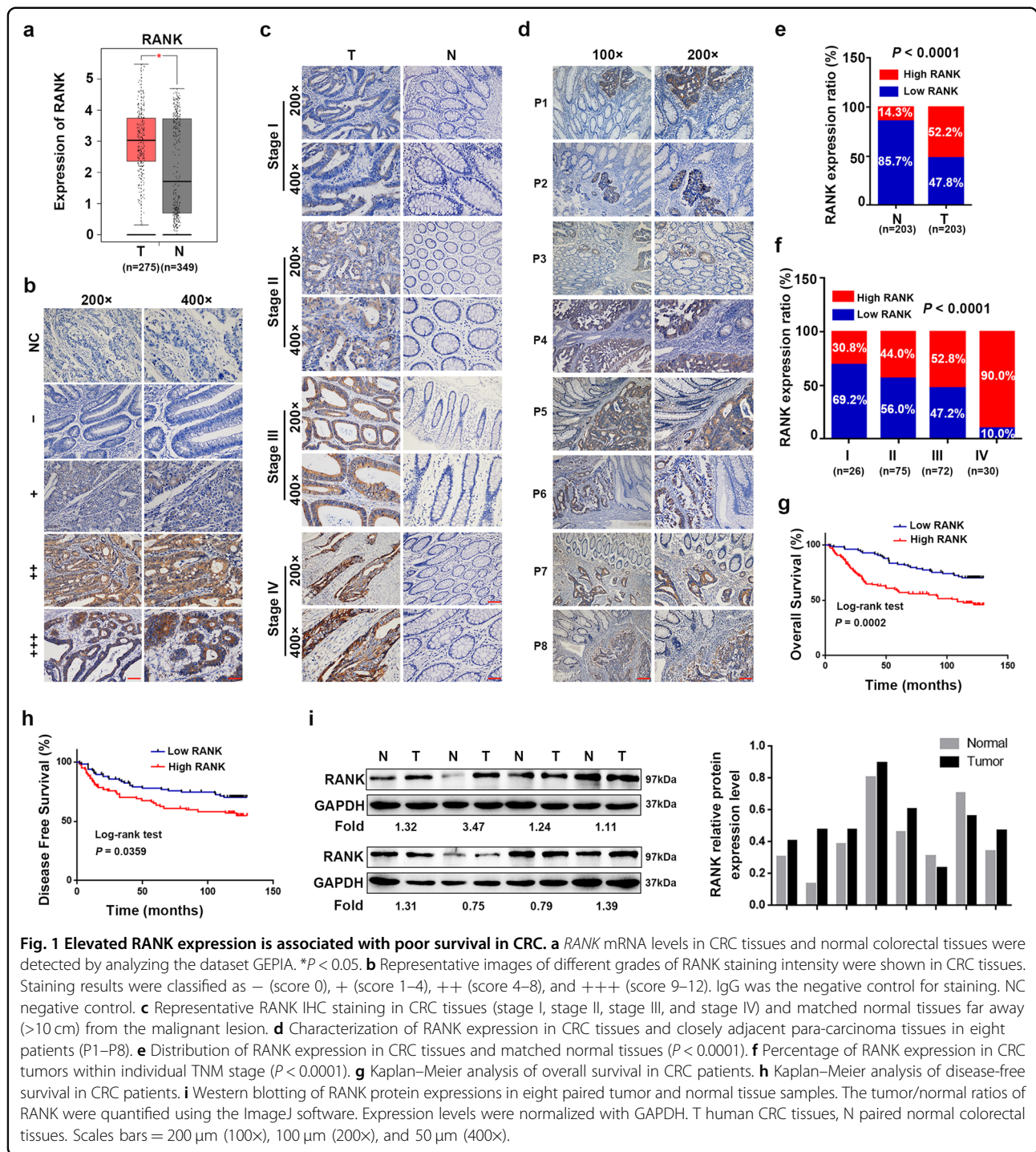
Results

RANK was increased in CRC and associated with worse prognosis

The GEPIA database showed that *RANK* mRNA levels were significantly increased in CRC tissues compared with those in normal colorectal tissues (Fig. 1a). Then, we used immunohistochemistry (IHC) staining to detect the expression of RANK in CRC. Representative images of different IHC staining grades of RANK are shown in Fig. 1b. RANK expression was upregulated in CRC tissues with different TNM stages compared with that in matched normal tissues distant (>10 cm) to the malignant lesion (Fig. 1c) or closely adjacent para-carcinoma tissues (Fig. 1d). As summarized in Fig. 1e, f, the proportion of high RANK expression significantly increased in CRC tissues than matched normal colonic epithelium ($P < 0.0001$) and increased gradually with the TNM stage ($P < 0.0001$). RANK expression was correlated prominently with worse clinicopathological parameters (Table 1). High RANK expression was associated markedly with decreased overall survival (OS; $P = 0.0002$) and disease-free survival ($P = 0.0359$; Fig. 1g, h). Moreover, univariate and multivariate survival analyses showed that RANK expression was an independent prognostic factor (Table 2) and recurrent factor (Table 3). Western blotting confirmed that RANK expression was upregulated in six (6/8, 75%) CRC samples compared with that in paired normal tissues (Fig. 1i). Taken together, RANK is frequently upregulated in CRC and is implicated in the pathogenesis or progression of CRC.

RANK promoted CRC migration and invasion in vitro and in vivo

To investigate the role of RANK in CRC, we first screened the mRNA levels of *RANK* in CRC cell lines from the CCLE database (Fig. S1a). We then measured the RANK protein levels in seven cell lines with different mRNA levels (Fig. 2a). According to protein levels, we transfected control LV-vector and LV-RANK to construct *RANK* stably overexpressing SW480 (SW480RK) and Caco2 (Caco2RK) cells (Fig. 2b and Fig. S1b, c). Meanwhile, two independent shRNAs against *RANK* were transfected into HT29 cells to establish *RANK* stable knockdown cells (Fig. 2c and Fig. S1d). *RANK* overexpression or combined with 100 ng/ml of RANKL promoted the migration and invasion of SW480 and Caco2 cells (Fig. 2d, e), whereas knockdown of *RANK* inhibited migration and invasion of HT29 cells (Fig. 2f). However,



RANK overexpression had no significant effect on the cell proliferation of CRC cell lines in either the absence or presence of RANKL (Fig. S1e, f). IHC staining showed that RANKL-positive cells exhibited the most similar distribution to CD3⁺CD25⁺FOXP3⁺ Treg cells in CRC tissues (Fig. S1g). The co-staining of CRC sections confirmed that RANKL and FOXP3 were colocalized (Fig.

S1h) consistent with previous study¹⁷. We furthermore proved that RANKL was colocalized with CD4, but was not in relation to CD68⁺ macrophages, CD8⁺ killer T cells, and T helper (Th) cell subsets for analyzing their critical lineage determining transcription factors, including T-bet (Th1), GATA3 (Th2), and RORγT (Th17; Figs. S2 and S3). In addition, although the endogenous RANKL

Table 1 Correlation between RANK expression and clinicopathologic features of 203 CRC patients.

Features	N of cases	RANK		P value (χ^2 tests)
		Low	High	
Total				
Age (years)				
<65	126	60	66	0.952
≥65	77	37	40	
Gender				
Male	125	62	63	0.512
Female	78	35	43	
Tumor size (cm)				
<5	173	93	80	<0.0001
≥5	30	4	26	
CEA level (ng/ml)				
≤5	62	27	35	0.423
>5	141	70	71	
Depth of invasion				
T1	2	0	2	0.015
T2	32	20	12	
T3	137	68	69	
T4	32	9	23	
Lymph node metastasis				
N0	115	63	52	0.027
N1	62	27	35	
N2	26	7	19	
Distant metastasis				
M0	173	94	79	<0.0001
M1	30	3	27	
TNM stage (AJCC)				
I	26	18	8	<0.0001
II	75	42	33	
III	72	34	38	
IV	30	3	27	

The bold number represents the P values with significant differences.

levels of CRC cells were very low (Fig. S4a), perturbation of endogenous RANKL by denosumab significantly attenuated migration and invasion of SW480RK and Caco2RK cells (Fig. S4b, c). These results indicated that baseline increase in migration and invasion was independent of exogenous RANKL, while low levels of endogenous RANKL are sufficient to elicit a metastatic phenotype in *RANK*-overexpressing CRC cells. In vivo

experiments showed that mice injected with SW480RK cells developed remarkably greater local invasion and distant metastasis compared with that in the control group (Fig. 2g, h). Bioluminescent imaging and hematoxylin and eosin (HE) staining of resected livers revealed that SW480RK significantly increased liver metastatic nodules (Fig. 2i–k). These results proved that *RANK* functionally contributed to the migration and invasion of CRC cells in vitro and to hepatic metastasis in vivo.

RANK regulated CRC migration and invasion by activating ACP5 expression

Increased basal levels of four canonical *RANK*-induced downstream pathways, phospho(p)-ERK1/2, p-P38, p-AKT, and p-NF κ B-P65 with or without *RANKL* time-dependent stimulation were observed in SW480RK and Caco2RK cells compared with those in the parental cells (Fig. S5a, b). Furthermore, we investigated whether *RANK* expressed on CRC cells displayed similar downstream signaling to osteoclasts and secreted osteoclast-specific genes to degrade surrounding tissue for metastasis. Interestingly, quantitative reverse transcription polymerase chain reaction (qRT-PCR) showed that *RANK* overexpression significantly increased the mRNA levels of osteoclast marker genes, *ACP5*, *CTSK* (cathepsin K), *MMP9* (matrix metalloproteinase 9), and *VCAM1* (vascular cell adhesion molecule 1) in SW480 and Caco2 cells (Fig. S5c). Conversely, *RANK* depletion reduced the expression of these genes in HT29 cells (Fig. S5d). Moreover, *ACP5* mRNA expressions were significantly increased in CRC tissues compared with that in normal colorectal tissues (Fig. S5e), and high *ACP5* expression decreased OS from online databases (Fig. S5f). These results were confirmed by related experimental analysis of patients with CRC¹⁸. Thus, we were prompted to explore whether *RANK* overexpression promoted CRC migration and invasion depending on *ACP5*. Western blotting showed that *RANK* overexpression significantly increased *ACP5* levels (Fig. 3a), whereas *RANK* depletion down-regulated *ACP5* levels in CRC cells (Fig. 3b). Silencing of *ACP5* in SW480RK and Caco2RK cells attenuated *RANK*-induced migration and invasion (Fig. 3c–e). Overexpression of *ACP5* could also rescue the reduction of HT29 cell migration and invasion induced by *RANK* silencing (Fig. 3f–h). Immunofluorescence confirmed that *ACP5* distribution within the tumor and stroma was more obvious in CRC tissues with high *RANK* expression than in those with low *RANK* expression (Fig. 3i). These results indicated that *ACP5* was critical for *RANK*-induced promotion of CRC migration and invasion.

RANK regulated ACP5 through the calcineurin/NFATC1 axis

Accumulating evidence suggests that some osteoclast-specific genes, including *ACP5*, are directly regulated by

Table 2 Univariate and multivariate analyses of prognostic parameters for overall survival in 203 CRC patients.

Prognostic parameter	Univariate analysis			Multivariate analysis		
	HR	95% CI	P value	HR	95% CI	P value
RANK expression (high vs. low)	2.323	1.480–3.647	<0.0001	2.144	1.357–3.387	0.001
Age (≥ 65 vs. < 65)	1.489	0.969–2.289	0.069	—	—	—
Gender (female vs. male)	1.007	0.650–1.561	0.974	—	—	—
CEA level (> 5 ng/ml vs. ≤ 5 ng/ml)	1.735	1.040–2.893	0.035	1.596	0.949–2.685	0.078
TNM stage (III/IV vs. I/II)	2.643	1.682–4.152	<0.0001	2.209	1.390–3.509	0.001

The bold number represents the *P* values with significant differences.
HR hazard ratio, *CI* confidence interval.

Table 3 Univariate and multivariate analyses of recurrent factors for disease-free survival in 173 CRC patients (stages I/II/III).

Prognostic parameter	Univariate analysis			Multivariate analysis		
	HR	95% CI	P value	HR	95% CI	P value
RANK expression (high vs. low)	1.718	1.036–2.848	0.036	1.685	1.010–2.814	0.046
Age (≥ 65 vs. < 65)	1.796	1.086–2.969	0.023	1.807	1.074–3.039	0.026
Gender (male vs. female)	0.943	0.564–1.576	0.822	—	—	—
CEA level (> 5 ng/ml vs. ≤ 5 ng/ml)	2.235	1.163–4.295	0.016	1.875	0.950–3.699	0.070
TNM stage (III vs. I/II)	1.859	1.124–3.075	0.016	1.764	1.040–2.994	0.035

The bold number represents the *P* values with significant differences.
HR hazard ratio, *CI* confidence interval.

NFATC1 (refs. 19,20). We next explored whether NFATC1 was involved in a downstream mechanism of RANK to regulate *ACP5* in CRC metastasis. High *NFATC1* expression was associated with worse OS or relapse-free survival in patients with CRC by analyzing the online databases (Fig. S6a–d). In addition, *RANK* mRNA expressions exhibited a strong positive correlation with *NFATC1* in patients with CRC in the indicated databases (Fig. S6e–g). QRT-PCR confirmed that the *NFATC1* mRNA levels were increased in SW480RK and Caco2RK cells, and decreased in *RANK* knockdown HT29 cells (Fig. S6h, i). NFATC1 undergoes efficient cytoplasmic dephosphorylation for nuclear translocation and facilitates its binding to downstream targets²¹. Western blotting demonstrated that *RANK* overexpression induced dephosphorylation of cytoplasmic NFATC1 and its nuclear translocation, while knockdown of *RANK* denoted the opposite results in CRC cells (Fig. 4a, b). Immunofluorescence also confirmed that *RANK* overexpression enriched NFATC1 levels in the nucleus, whereas *RANK* silencing had the opposite effect (Fig. 4c, d). Furthermore, increased nuclear NFATC1 levels were observed in high *RANK* expression CRC tissues compared with those in

matched normal tissues and tumor tissues with negative *RANK* expression, as revealed by immunofluorescence staining (Fig. 4e). We then investigated whether *RANK* upregulated *ACP5* expression to promote metastasis depending on NFATC1 in CRC. The online datasets showed that *NFATC1* mRNA expressions directly correlated with *ACP5* expression in patients with CRC (Fig. 4f–h). In addition, CHIP-seq datasets from ENCODE²² showed that NFATC1 and other transcription factors, such as MITF, PU.1, and AP-1 were all enriched on the *ACP5* promoter (Fig. 4i). These transcription factors have been proven to interact with the *ACP5* promoter and activate its expression^{19,20,23,24}. In our study, we confirmed that silencing of *NFATC1* in SW480RK or Caco2RK cells decreased *ACP5* expression significantly (Fig. 4j), and attenuated *RANK*-induced migration and invasion (Fig. 4k, l). These results revealed that NFATC1, activated by *RANK*, specifically occupied the *ACP5* promoter to regulate the migration and invasion of CRC cells.

Notably, calcineurin, as a direct upstream regulator of NFATC1, dephosphorylates NFATC1 and initiates its nuclear translocation²¹. Thus, we further tested whether the inhibition of calcineurin had an effect on *RANK*-induced

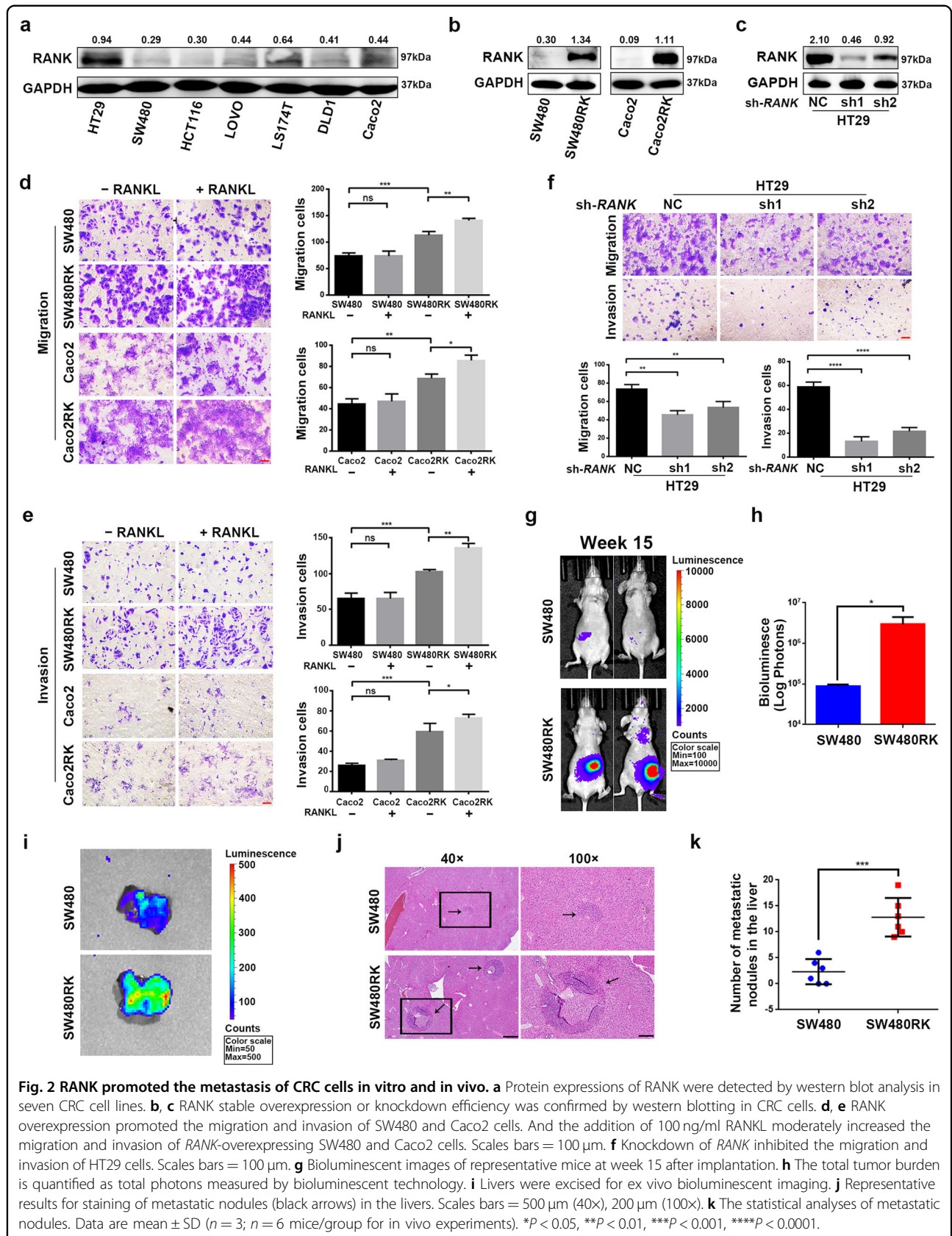
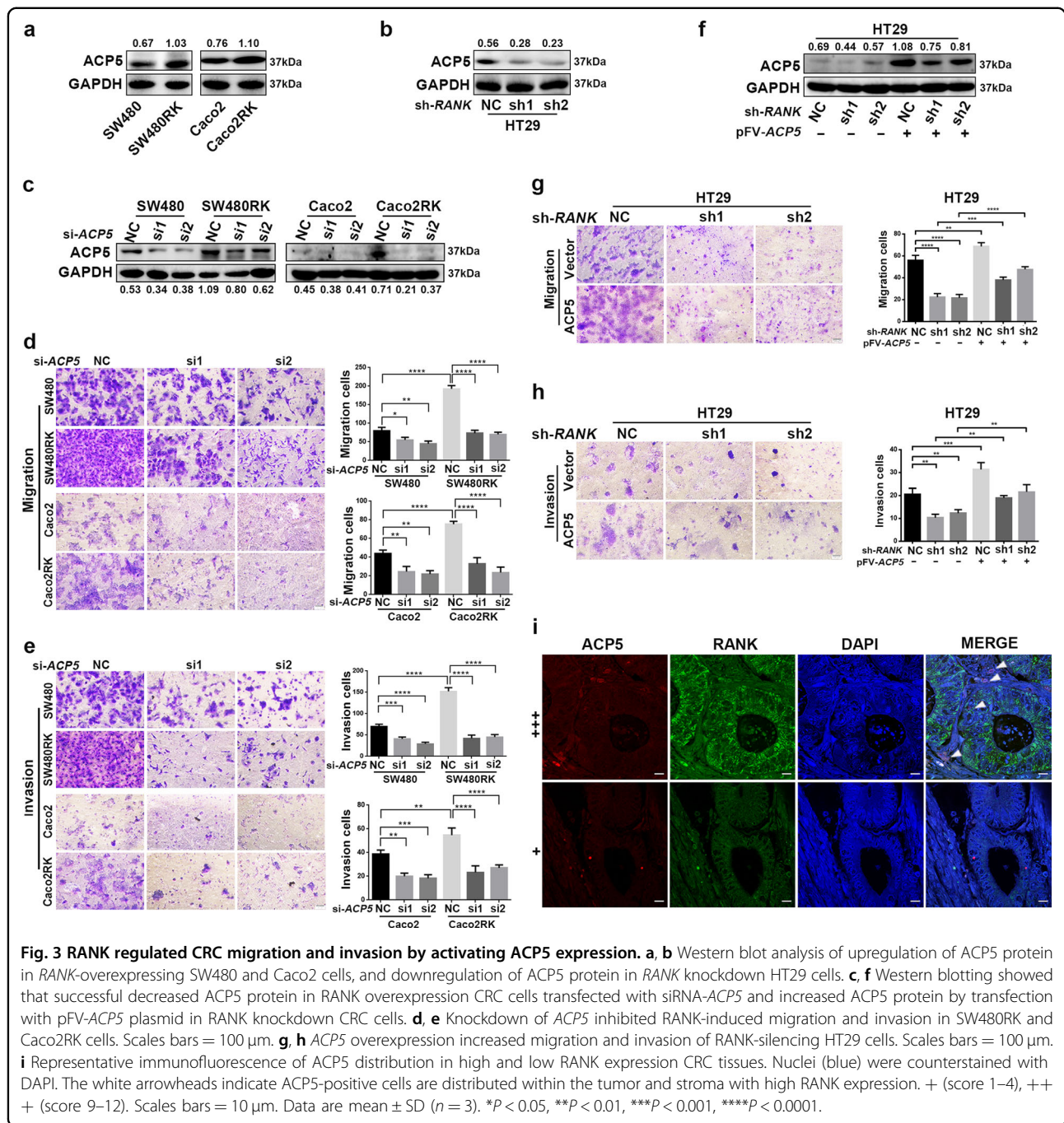


Fig. 2 RANK promoted the metastasis of CRC cells in vitro and in vivo. **a** Protein expressions of RANK were detected by western blot analysis in seven CRC cell lines. **b, c** RANK stable overexpression or knockdown efficiency was confirmed by western blotting in CRC cells. **d, e** RANK overexpression promoted the migration and invasion of SW480 and Caco2 cells. And the addition of 100 ng/ml RANKL moderately increased the migration and invasion of RANK-overexpressing SW480 and Caco2 cells. Scales bars = 100 μ m. **f** Knockdown of RANK inhibited the migration and invasion of HT29 cells. Scales bars = 100 μ m. **g** Bioluminescent images of representative mice at week 15 after implantation. **h** The total tumor burden is quantified as total photons measured by bioluminescent technology. **i** Livers were excised for ex vivo bioluminescent imaging. **j** Representative results for staining of metastatic nodules (black arrows) in the livers. Scales bars = 500 μ m (40x), 200 μ m (100x). **k** The statistical analyses of metastatic nodules. Data are mean \pm SD ($n = 3$; $n = 6$ mice/group for in vivo experiments). * $P < 0.05$, ** $P < 0.01$, *** $P < 0.001$, **** $P < 0.0001$.



migration and invasion in CRC. Treatment with the calcineurin inhibitor cyclosporin A (CsA) gradually attenuated the migration and invasion of SW480RK and Caco2RK cells at 1, 5, and 10 μg/ml (Fig. 5a, b). Immunofluorescence and western blotting and showed that 10 μg/ml CsA decreased NFATC1 nuclear translocation significantly in SW480RK and Caco2RK cells (Figs. 4c and 5c). In addition, 10 μg/ml CsA reversed the upregulation of ACP5 protein levels in SW480RK and Caco2RK cells (Fig. 5d). Collectively, our results demonstrated that RANK overexpression activated

ACP5 expression through calcineurin/NFATC1 signaling, which eventually induced metastasis in CRC.

RANK activated the calcineurin/NFATC1 axis via Ca²⁺ oscillation

Ca²⁺ oscillation is essential to maintain NFATC1 in the nucleus and enables transcriptional activation of NFATC1 (ref. 25). To explore the impact of Ca²⁺ signaling on RANK-induced NFATC1 activation, we first evaluated cytoplasmic Ca²⁺ oscillation in CRC cells. Calcium-flux

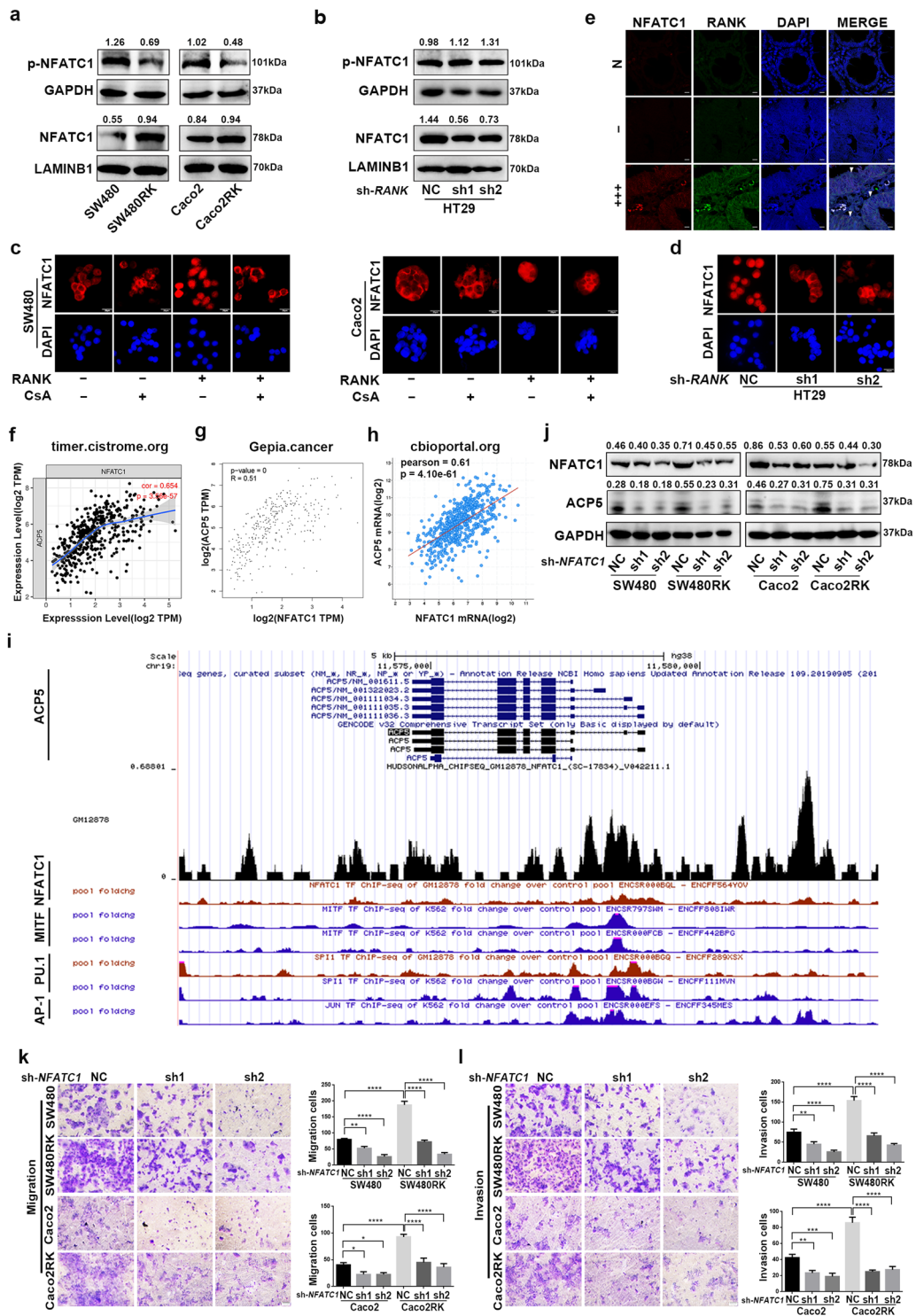


Fig. 4 (See legend on next page.)

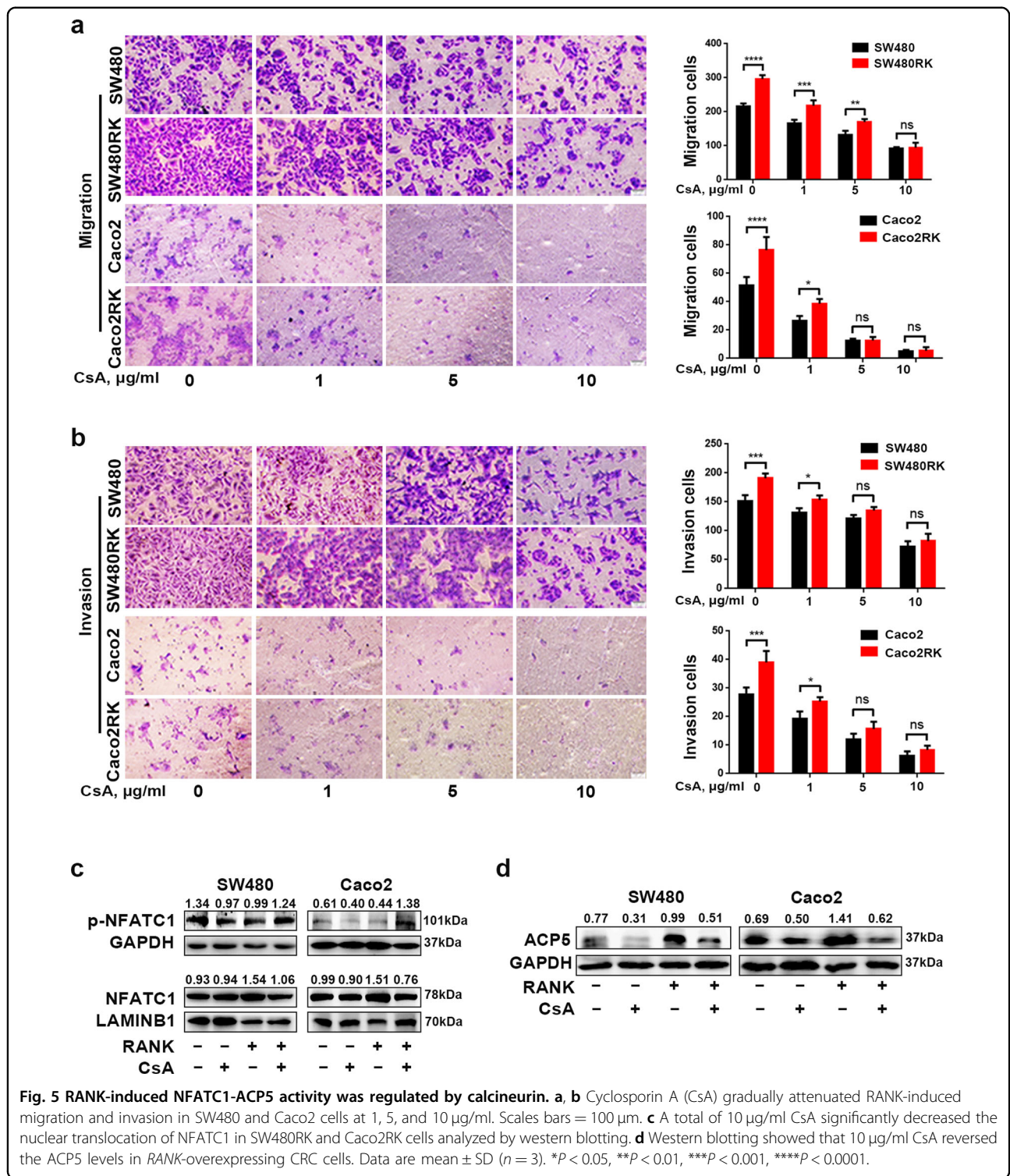
(see figure on previous page)

Fig. 4 RANK upregulated ACP5 expression through driving NFATC1 nuclear translocation. **a, b** Western blotting analyzed the protein levels of phosphorylated NFATC1 and NFATC1 in cytoplasm, and nucleus of *RANK*-overexpressing or knockdown CRC cells. GAPDH served as the cytoplasmic control and lamin B1 as the nuclear protein loading control. **c** Immunofluorescence staining of subcellular localization of NFATC1 in *RANK* overexpression and control cells with or without treatment of 10 $\mu\text{g/ml}$ cyclosporin A (CsA). Scales bars = 20 μm . **d** Representative immunofluorescence of subcellular localization of NFATC1 in *RANK*-depleted HT29 cells. Scales bars = 20 μm . **e** The NFATC1 subcellular localization in matched normal tissues, negative and high *RANK* expression of CRC tissues by immunofluorescence staining. DAPI (nuclei, blue). *RANK* is visualized in the membranes and in the cytoplasm surrounding the nucleus of the NFATC1 in CRC tissues (white arrowheads). – (score 0), +++ (score 9–12). N paired normal colorectal tissues. Scales bars = 10 μm . **f–h** Correlation analysis between mRNA levels of *NFATC1* and *ACP5* from indicated online datasets. **i** ChIP-seq data showed a UCSC Genome Browser screenshot of the *ACP5* promoter region for *NFATC1* and *SPI1* in GM12878 cells and *MITF*, *SPI1*, and *JUN* in K562 cells from ENCODE. **j** *NFATC1* knockdown reversed *RANK*-induced *ACP5* expression. **k, l** Silencing of *NFATC1* decreased *RANK*-induced migration and invasion in SW480 and Caco2 cells. Scales bars = 100 μm . Data are mean \pm SD ($n = 3$). * $P < 0.05$, ** $P < 0.01$, *** $P < 0.001$, **** $P < 0.0001$.

measurement showed that overexpression of *RANK* in SW480, and Caco2 cells increased cytoplasmic Ca^{2+} levels and Ca^{2+} influx significantly (Fig. 6a). The opposite results were observed in *RANK* knockdown HT29 cells (Fig. 6b). Store-operated Ca^{2+} entry (SOCE) is a major mechanism to increase cytosolic Ca^{2+} influx and has been reported to be associated with cancer malignancy in CRC cells^{26,27}. The *STIM1*, *ORAI* calcium release-activated calcium modulator 1 (*ORAI1*), and canonical transient receptor potential channel 1 (*TRPC1*) protein families are the main modulators of SOCE^{27,28}. We found that the mRNA levels of *STIM1*, *ORAI1*, and *TRPC1* were upregulated significantly in SW480RK and Caco2RK cells, and downregulated in *RANK* knockdown HT29 cells (Fig. S7a, b). *STIM1*, as the endoplasmic reticulum (ER) Ca^{2+} sensor for SOCE, migrates from the ER to the plasma membrane to activate Ca^{2+} influx by SOCE^{29,30}. *STIM1* overexpression promotes CRC metastasis, and is associated with progression and poor prognosis in CRC^{31,32}. Thus, we analyzed whether *STIM1* was a downstream factor of *RANK* to regulate the calcineurin/NFATC1 axis. We found that the mRNA expressions of *RANK* correlated positively with *STIM1* in patients with CRC by analyzing database GEPIA (Fig. S7c). Western blotting confirmed that *RANK* overexpression induced *STIM1* upregulation and *RANK* knockdown reduced *STIM1* expression in CRC cells (Fig. 6c, d). Immunofluorescence staining further confirmed that strong cytoplasmic *STIM1* staining was detected in high *RANK* expression CRC tissues, while weak *STIM1* staining was observed in matched normal epithelial tissues with low *RANK* expression (Fig. 6e). Moreover, the online datasets showed that the *STIM1* mRNA levels correlated positively with *NFATC1* and *ACP5* levels in patients with CRC (Fig. 6f–h and Fig. S7d–f). Consistently, silencing of *STIM1* by small interfering RNA (siRNA) transfection inhibited the reduction of cytoplasmic phosphorylated NFATC1, and *ACP5* activation induced by *RANK* overexpression (Fig. 6i). The rescue experiment revealed that silencing *STIM1* downregulated the migration and invasion of SW480RK and Caco2RK cells (Fig. 6j, k). These results indicated that

the *STIM1*- Ca^{2+} signaling pathway is involved in the *RANK*-induced activation of the calcineurin/NFATC1-*ACP5* axis and metastasis.

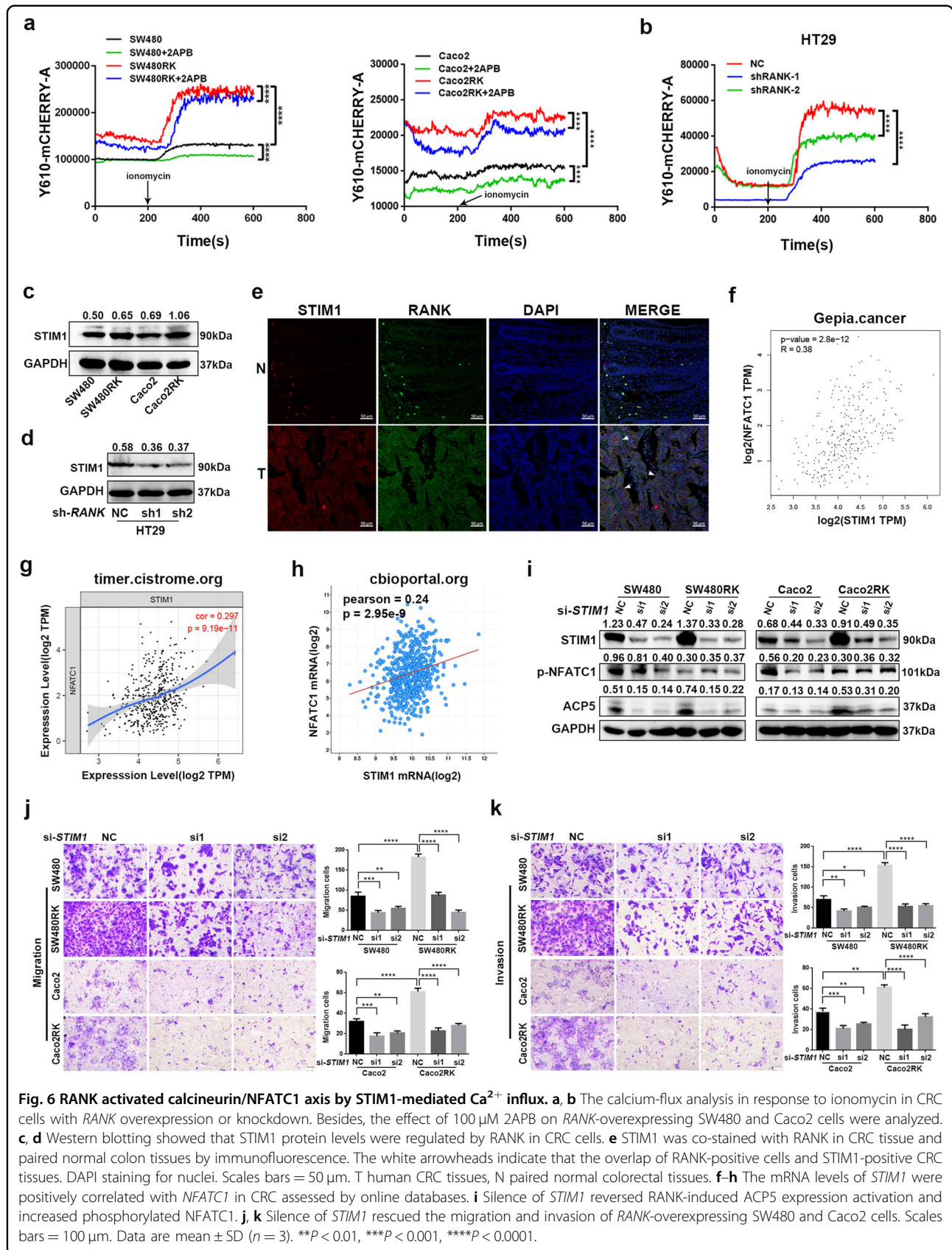
PLC γ -mediated IP3 production and subsequent activation of ER Ca^{2+} release play a substantial role in osteoclast differentiation³³. The indicated online datasets showed that mRNA levels of *RANK* were positively correlated with *IP3R* and *PLC γ* in patients with CRC (Fig. S8a–d). We supposed that *RANK* upregulated cytosolic Ca^{2+} concentration in CRC through ER Ca^{2+} release via PLC γ -mediated IP3 production, as well as by Ca^{2+} influx dependent on *STIM1*. To validate this, the effect of the IP3R antagonist, 2-aminoethoxydiphenyl-borate (2APB) on Ca^{2+} oscillation was assessed. We found that pretreatment with 100 μM 2APB could attenuate the cytosol Ca^{2+} concentration at both basal and *RANK* overexpression stimulatory level in CRC cells (Fig. 6a). Western blotting showed that 2APB prevented NFATC1 cytoplasmic dephosphorylation and nuclear translocation in SW480RK and Caco2RK cells (Fig. 7a). The 2APB-induced reversal of significantly nuclear translocation in *RANK*-overexpressing CRC cells was also confirmed by immunofluorescence (Fig. 7b). Furthermore, 2APB could rescue *RANK*-induced migration and invasion in SW480 and Caco2 cells (Fig. 7c, d). The mRNA expressions of *IP3R* were found to have positive correlation for *PLC γ* in patients with CRC by analyzing the online datasets (Fig. 7e–g). Next, we examined the effect of inhibition of PLC γ on *RANK*-induced activity of CRC cells. Western blotting showed that the PLC γ inhibitor U73122 reversed NFATC1 nuclear translocation, and *ACP5* upregulation in SW480RK and Caco2RK cells (Fig. 7h). Notably, U73122 decreased the protein levels of *STIM1* significantly in *RANK*-overexpressing CRC cells, indicating that PLC γ -mediated IP3 also regulates the activity of SOCE (Fig. 7h). The online databases also confirmed that mRNA expressions of *IP3R* correlated positively with *STIM1* in patients with CRC (Fig. S8e–g). Furthermore, U73122 significantly attenuated the migration and



invasion of SW480RK and Caco2RK cells (Fig. 7i, j). The above results revealed that RANK induced the calcineurin/NFATC1 axis by activation of PLCγ-IP3-STIM1-mediated ER Ca²⁺ release and Ca²⁺ influx.

Discussion

Approximately 25% of patients with CRC present with metastases at initial diagnosis and almost 50% ultimately develop metastases, leading to the high mortality rates



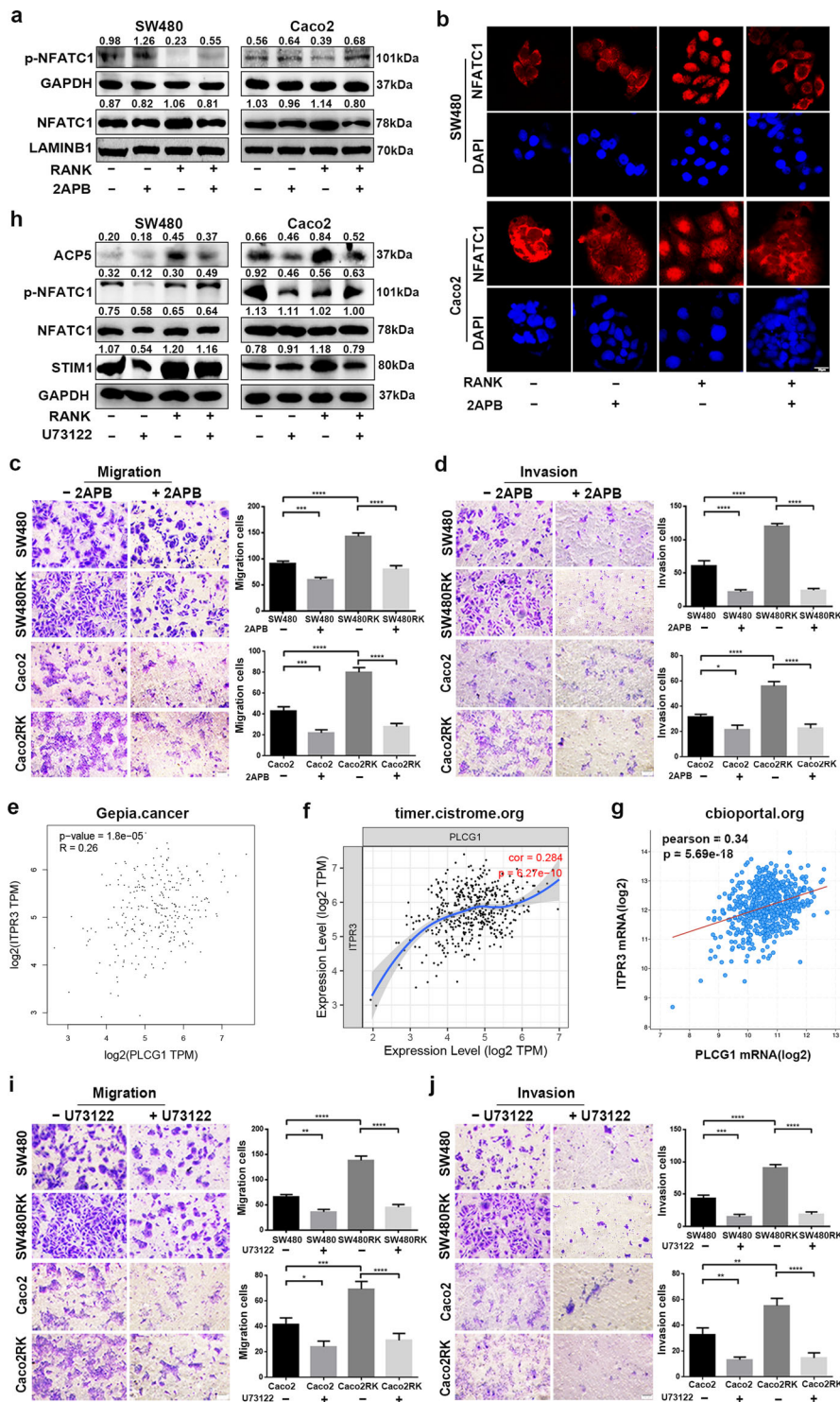


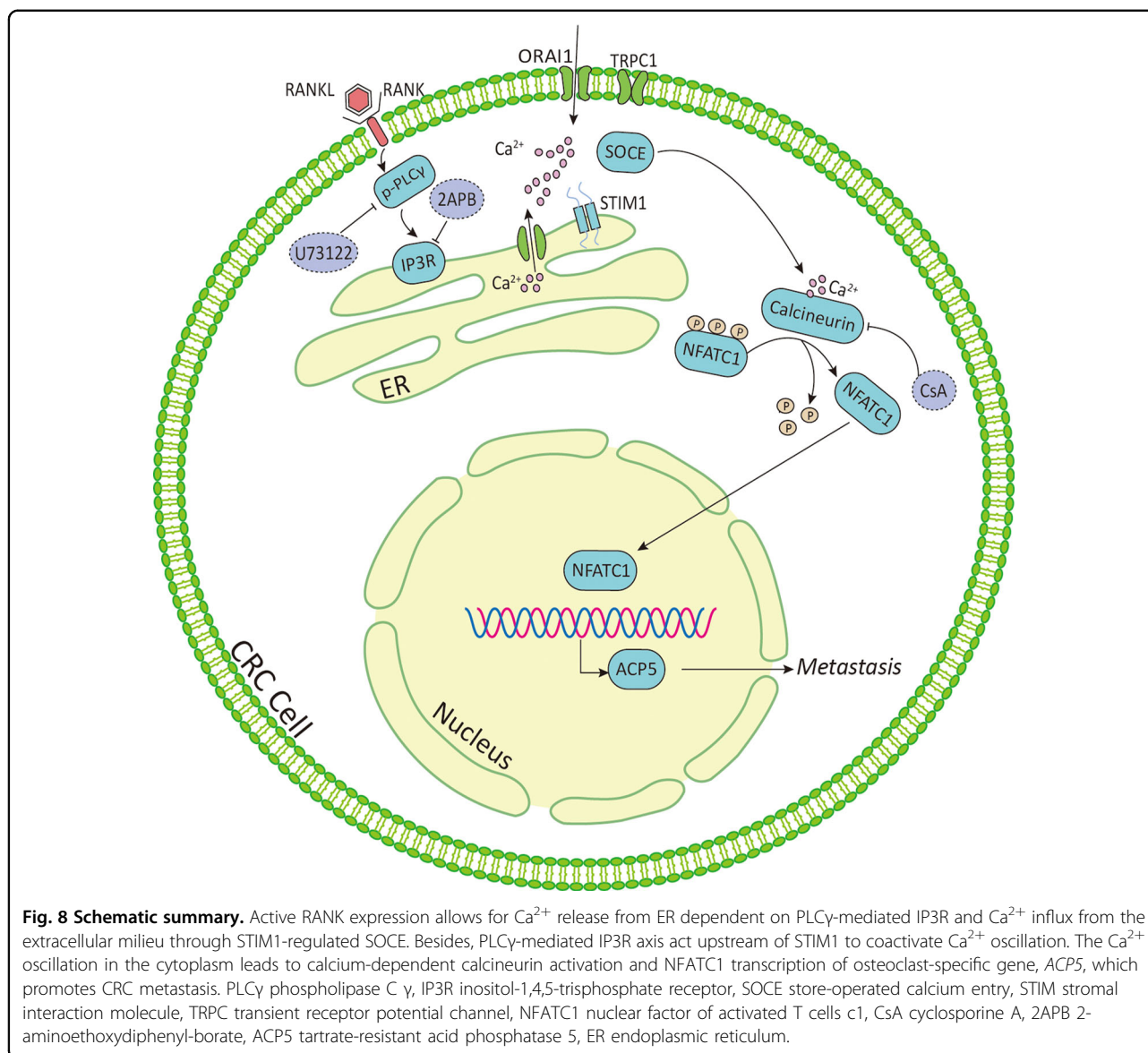
Fig. 7 RANK induced STIM1-mediated Ca^{2+} influx and ER Ca^{2+} release by activating the PLC γ -IP3R axis. **a** Western blotting analyzed the protein levels of NFATC1 and phosphorylated NFATC1 in nuclear and cytoplasm of 100 μM 2APB-treating CRC cells. **b** Immunofluorescence staining showed nucleocytoplasmic localization of NFATC1 in CRC cells treated by 100 μM 2APB. Blue represents DAPI staining. Scales bars = 20 μm . **c, d** A total of 100 μM 2APB rescued RANK-mediated migration and invasion of SW480 and Caco2 cells. Scales bars = 100 μm . **e-g** Scatter plots showed the significant positive relationship between mRNA expressions of *IP3R* and *PLC γ* obtained by online datasets. *PLCG1*, *PLC γ* , *ITPR3*, *IP3R*. **h** A total of 10 μM U73122 rescued the protein levels of STIM1, ACP5, and the phosphorylation level of NFATC1 in SW480RK and Caco2RK cells. **i, j** Representative images of CRC cells treated by 10 μM U73122 subjected to the transwell migration and invasion assays. Scales bars = 100 μm . Data are mean \pm SD ($n = 3$). * $P < 0.05$, ** $P < 0.01$, *** $P < 0.001$, **** $P < 0.0001$.

observed in CRC³⁴. Despite improvements in therapeutic early-stage CRC over past decades, no effective therapy is currently available for advanced or metastatic CRC for poor understanding of the mechanisms underlying CRC metastasis³⁵. In the present study, we found higher RANK expression in CRC tissues compared with that in matched normal tissues, which correlated with worse prognosis. Furthermore, RANK expressed in CRC-activated PLC γ -mediated IP3 signaling to evoke Ca²⁺ release from the ER, and upregulated STIM1 to promote Ca²⁺ influx through SOCE, which cooperate to generate Ca²⁺ oscillation. In addition, STIM1 was also regulated by PLC γ induction. RANK-mediated intracellular Ca²⁺ mobilization subsequently stimulated calcineurin to dephosphorylate NFATC1 and induce NFATC1 nuclear translocation. In the nucleus, NFATC1 transcriptionally upregulates osteoclast-specific gene *ACP5* to promote the migration and invasion of CRC (Fig. 8), indicating that RANK might serve as a potential therapeutic target.

To the best of our knowledge, this study is the first to report functional RANK expression in CRC. Jones et al.⁴ first mentioned the relationship between RANK and metastasis in CRC cells. Their study showed that the human CRC cell lines SW480 and Colo205 had no detectable levels of RANK. These CRC cells failed to migrate when induced by RANKL and metastasized into the bones after intracardiac injection. Thus, for a long time afterward, research associated with RANK in cancer mainly focused on breast and prostate cancer, which frequently develop bone metastasis. RANK also has a role in other cancers, such as osteosarcoma³⁶ and melanoma³⁷; however, there have been few studies in CRC. This might be explained by the fact that RANK is related to the bone environment, whereas CRC mainly develops liver metastasis, not bone metastasis, like breast and prostate cancer. Although one study mentioned that 75% of CRC tissues were RANK-positive⁹ and scattered reports showed that the role of RANK in CRC was related to the bone environment or osteoclast activity^{14–16}, the direct function of RANK in CRC is still unknown. In this work, we clearly demonstrated positive immunostaining of RANK in CRC tissues, and confirmed high RANK expression in the CRC cell line HT29 and its low expression in SW480 and Caco2 cells. These results were similar to those reported by previous studies^{4,9}. In addition, we found that RANK expression correlated negatively with the prognosis of patients with CRC. Gain and loss of function studies showed that RANK promoted the migration and invasion of CRC cells. Overexpression of RANK in CRC cells resulted in constitutive activation of the canonical downstream signaling pathway (p-P65, p-P38, p-AKT, and p-ERK). Moreover, presence of RANKL

significantly increased the basal levels of these RANK downstream targets. Thus, our results clearly demonstrated that overexpression of RANK led to RANKL-dependent and RANKL-independent activation of downstream pathways, as described in other cancers^{4,13}. Interestingly, we found that tumor-infiltrating CD25⁺FOXP3⁺Treg cells were the major producers of RANKL within the microenvironment of RANK-expressing CRC, which may provide a reference for the treatment of CRC metastasis. Taken together, our study proved that RANK expressed in CRC is functional.

Overexpression of RANK promoted CRC metastasis by activating the Ca²⁺-calcineurin/NFATC1-ACP5 axis. Previous studies have proven that osteoclast-associated signaling molecules promote CRC metastatic capacity, notably the transcription factor NFATC1 and its regulation by calcineurin^{38,39}. Questions concerning which factor activates the calcineurin/NFATC1 axis in CRC and how calcineurin/NFATC1 regulates CRC metastasis remain unanswered. In the present study, we found that PLC γ -IP3-mediated ER Ca²⁺ release and STIM1-regulated Ca²⁺ influx through SOCE acted together to activate calcineurin/NFATC1 in RANK-overexpressing CRC cells. Moreover, we found that STIM1 was also regulated by PLC γ , indicating that PLC γ -IP3 signaling and STIM1 were involved closely in the Ca²⁺ oscillation induced by RANK in CRC. After being activated, calcineurin enhances NFATC1 activity by dephosphorylating it, thus increasing NFATC1's nuclear translocation. NFATC1 further activates the transcription of the osteoclast-specific gene, *ACP5*. *ACP5* is a metalloenzyme of the acid phosphoprotein phosphatase family⁴⁰ and the major function of *ACP5* in bone resorption is the catabolic degradation of bone matrix phosphoproteins. *ACP5* has been recommended as a serum marker for bone resorptive activity in pathological states, such as osteoporosis and notably, bone metastasis of cancers^{41,42}. Previous studies revealed that high *ACP5* expression correlated with reduced survival and increased metastasis in various cancers^{43–45}. In addition, *ACP5* has been proven to aggravate the proliferation and invasion of CRC cells and might serve as an indicator for poor prognosis in CRC¹⁸. Consistently, our research also showed that RANK-induced *ACP5* affected the NFATC1 pathway to promote the migration and invasion of CRC cells significantly. These results support a role for RANK in the regulation of CRC metastasis and provide novel insights into the molecular pathways linking RANK expressed in CRC to osteoclast differentiation signaling. Therefore, inhibition of osteoclastogenesis signaling not only interrupts the vicious cycle between bone and CRC, but also more importantly, it directly decreases the



metastatic ability of CRC with high RANK expression. Moreover, these results implied that OPG and denosumab, the drugs that block RANKL–RANK interaction, are not sufficient to suppress CRC bone metastasis and skeletal-related events (SREs). Drugs targeting the Ca^{2+} -calcineurin/NFATC1-ACP5 axis in RANK-expressing CRC might be needed, such as the inhibitors CsA, 2APB, and U73122 used in the present study.

There were several limitations of this study. Although CRC metastasis was independent of exogenous RANKL, the presence of RANKL could enhance RANK-overexpressing CRC metastasis and RANK signaling activation. Our IHC staining found that RANKL might be derived from tumor-infiltrating $\text{CD}25^+\text{FOXP}3^+$ Treg cells. Further experiments are needed to verify the exact source of RANKL to better

determine the role of the RANK–RANKL system in CRC. In addition, it remains to be determined how RANK initially activates PLC γ to induce the Ca^{2+} -calcineurin/NFATC1 axis, which will require further mechanistic experiments.

In conclusion, our findings demonstrated that RANK is upregulated in CRC and correlates with poor outcomes in patients with CRC. In addition, we determined a novel role of RANK expression in promoting CRC metastasis in vitro and in vivo. Mechanistically, in CRC, RANK induces PLC γ -IP3R-STIM1 signaling-mediated Ca^{2+} oscillation and further activated the calcineurin/NFATC1-ACP5 pathway to regulate CRC metastasis. This axis linking RANK to osteoclast-specific gene *ACP5* might provide promising targets to develop antimetastatic agents to treat patients with CRC.

Materials and methods

Patients and tissue specimens

A total of 203 pairs of CRC and nontumor colonic epithelium paraffin-embedded tissues were obtained from operated patients at The First Affiliated Hospital, Sun Yat-sen University (Guangzhou, China) from 2008 to 2011. Follow-ups of these 203 patients ended on December 1st, 2019. The follow-up duration ranged from 2 to 130 months. The fresh CRC and matched normal tissues were collected from operated patients at The Seven Affiliated Hospital, Sun Yat-sen University (Shenzhen, China). Patients who underwent preoperative chemotherapy and/or radiotherapy were excluded. Each patient provided written informed consent. The use of clinical samples was approved by the Ethics Committee of Sun Yat-sen University.

Antibodies and reagents

Primary antibodies used in this study included: anti-RANK (ab13918), anti-FOXP3 (ab20034), anti-CD3 (ab16669), anti-CD19 (ab134114), anti-rabbit RANKL (ab9957), anti-CD25 (ab128955), anti-CD4 (ab133616), anti-CD8 (ab4055), and anti-CD68 (ab201340) from Abcam; anti-ERK (#9102), anti-p-ERK (Thr202/Tyr204; #9101), anti-P38 (#9212), anti-p-P38 (Thr180/Tyr182; #9211), anti-P65 (#4764), anti-p-P65 (Ser536; #3033), anti-AKT (#9272), and anti-p-AKT (Ser473; #9101) from CST; anti-IgG isotype control (10500 C) from Thermo; anti-GAPDH (60004-1-Ig), anti-STIM1 (11565-1-AP), GATA3 (66400-1-Ig), and anti-mouse RANKL (66610-1-Ig) from Proteintech, Wuhan, China; anti-ACP5 (DF6989), anti-rabbit ROR γ (DF3196), and anti-T-bet (DF7759) from Affinity Biosciences, OH, USA; anti-mouse ROR γ (sc-365476) from Santa Cruz, CA, USA; and anti-lamin B1 from (AF1408, Beyotime, Beijing, China). The reagents included: CsA, U73122, 2APB, and ionomycin from MCE; RANKL, EGF, and bFGF from PeproTech; and denosumab from TheraMabs (Shanghai, China).

Immunohistochemistry

After routine deparaffinization and rehydration, treatment with hydrogen peroxide, antigen retrieval, and blocking with goat serum, the tissue sections were incubated with primary antibodies overnight at 4 °C. Rabbit IgG was used as negative control. All antibodies were diluted according to the instructions. Next, the slides were incubated with secondary antibody, stained with diaminobenzidine tetrahydrochloride (DAKO, Carpinteria, CA), and counterstained with hematoxylin. The IHC staining was analyzed by two independent pathologists who were blinded to the patient's clinical parameters. The staining intensity was documented as 0 (no staining), 1 (weak immunoreactivity),

2 (moderate immunoreactivity), and 3 (strong immunoreactivity). The percentage of immunoreactive cells was scored as 0 (no positive cells), 1 (<20%), 2 (20–50%), 3 (51–75%), and 4 (>75%). The final score was determined by multiplying the intensity and the percentage of immunoreactive cells. Depending on the final score, the staining results were graded as – (score 0), + (score 1–4), ++ (score 5–8), and +++ (score 9–12). The grade was furthermore defined as low expression (–, +) and high expression (++, +++)^{46,47}.

Cell lines and culture conditions

Human CRC cell lines SW480, Caco2, HT29, DLD1, HCT116, LS174T, and LOVO were purchased from the American Type Culture Collection. All cells were authenticated and free of mycoplasma. HT29 were cultured in RPMI 1640 Medium (Gibco), and the other cell lines were maintained in Dulbecco's modified Eagle's medium (Gibco) at 37 °C with 5% CO₂. Medium was added with 10% fetal bovine serum (FBS; Gibco) for cell culture.

Cell lines transfection

For transient transfection, two independent siRNA duplexes against *STIM1*, *ACP5*, and control siRNA, overexpression plasmids including pFV155-GFP-puro-*ACP5* and control vector were introduced into cells using Lipofectamine 3000 reagent (Invitrogen), according to the manufacturer's instructions. For stable overexpression and knockdown transfection, 293T cells were transfected with pFV155-GFP-puro-*RANK*, pLKO.1-puro-*RANK*-target shRNA, PTSB-NEO-*NFATC1*-target shRNA, and their empty vectors using package plasmids and polyethyleneimine (Polysciences). Virus particles were harvested 48 h after transfection and used for cell infection with polybrene (Sigma). Puromycin (Sigma) and G418 (Sigma) were used for puro-resistance and NEO-resistance plasmids, respectively. All siRNA duplexes, shRNA constructs, and overexpressing plasmids were from Transheep (Shanghai, China). The siRNA and shRNA sequences are listed in Supplementary Tables S1 and S2.

Western blot analysis

Briefly, proteins from total cell lysates (20 μ g) were separated by SDS-PAGE, transferred onto polyvinylidene difluoride membranes (Millipore), and immunoblotted with the indicated antibodies, followed by peroxidase-conjugated anti-mouse or rabbit IgG. Anti-GAPDH antibody was diluted at 1:10,000 and other primary antibodies were 1:1000. Nuclear and Cytoplasmic Protein Extraction kit (Beyotime, Beijing, China) was used to separate the nuclear and cytoplasmic protein, according to the manufacturer's

protocol. Membranes were finally infiltrated by an enhanced chemiluminescence reagent and visualized using Chemiluminescence imaging Systems (Bio-Rad).

Quantitative reverse transcription polymerase chain reaction

Total RNA was extracted from cells using AG RNAex Pro Reagent (AG21102, ACCURATE BIOTECHNOLOGY, Hunan, China), according to the manufacturer's protocol. Reverse transcription was performed using the Evo M-MLV RT Premix (AG11706, ACCURATE BIOTECHNOLOGY, Hunan, China). The qRT-PCR assay was performed using SYBR[®] Green Premix Pro Taq HS qPCR Kit (AG11701, ACCURATE BIOTECHNOLOGY, Hunan, China) in the CFX96 Touch Real-Time PCR system (CFX96, BIO-RAD Laboratories, Hercules, USA). *GAPDH* was used as an endogenous reference to normalize RNA expression. The primer sequences used are listed in Supplementary Table S3.

Migration and invasion assays

A total of 2×10^5 cells in serum-free medium were seeded into the upper chamber of inserts (8 μ m pore size, BD Biosciences, USA) with or without diluted Matrigel (Corning, USA) for migration and invasion in 24-well plates. Besides, the indicated concentration of chemicals used in this study was added into the upper chambers to evaluate their effect. Medium supplemented plus 20% FBS was used as a chemoattractant in the lower chambers. After 60-h incubation, the cells on the lower membrane were fixed and stained with crystal violet. The staining cells were randomly imaged in eight different fields with a microscope.

Cell proliferation assay

A total of 1000 cells were inoculated into 96-well plates with complete medium. Four consecutive days after initial planting, cells were incubated in the medium with 10% Cell Counting Kit-8 (Dojindo, Japan) for 2 h at 37 °C in dark. The cell absorbance was then detected at 450 nm with a microplate reader (Synergy H1M, BioTek).

Immunofluorescence

Cells were seeded onto sterile slides into 24-well culture plates. After reached a suitable confluence, cells were fixed with 4% paraformaldehyde, permeabilized with 0.1% Triton/PBS, and blocked with goat serum. The methods for tissue slices before primary antibody incubation were the same as IHC.

Next, cells were incubated with indicated primary antibody overnight at 4 °C. For double immunofluorescence of tissue slices, both primary antibodies were mixed and incubated. All antibodies were used according

to the instructions. On the second day, cells or slices were further incubated with Alexa Fluor 488 goat anti-mouse IgG (A-11001, Thermo) or Alexa Fluor 594 goat anti-rabbit IgG (A-11012, Thermo), stained with DAPI (Sigma) label nuclei, and finally observed under Leica fluorescence or Zeiss confocal microscopy.

Animal experiments

Female 6-week-old BABL/c nude mice were purchased from Beijing Vital River Laboratory Animal Technology Company (Beijing, China). All animal experiments were approved by the Sun Yat-sen University Institutional Animal Care and Use Committee. The mice were randomly allocated into two groups ($n=6$) and received intrasplenic transplantation to study liver metastasis. For the spleen injection, the mice were anesthetized with isoflurane and laparotomized to expose the spleen. A total of 1.5×10^6 SW480-Luc/Control or SW480-Luc/RANK cells in 50 μ l PBS were slowly injected into the spleen using an insulin syringe. The spleen was then replaced into the abdomen cavity and the abdominal wall was sutured. Liver metastasis was determined by bioluminescence imaging using the IVIS Imaging System (Xenogen). After 15 weeks, the mice were euthanized and the livers were removed for bioluminescence imaging and HE staining to confirm metastatic foci. The statistical analyses were performed by researchers blinded to experiment design.

Calcium-flux measurements

Cells were trypsinized and incubated with 10 μ M Calbryte[™] 630 AM Esters (AAT Bioquest) for 1 h at room temperature, according to instruction. Then, cells were switched to Hanks and Hepes buffer containing 2 mM Ca^{2+} , and subjected to FACS analysis by a CytoFLEX flow cytometer (Beckman) to measure fluorescence intensity. During the FACS analysis, cells were stimulated with ionomycin (2 μ g/ml). The results were further quantitatively analyzed by FlowJo (v10) software.

Bioinformatics analysis

The gene expression data and Kaplan–Meier survival plots for CRC patients were appraised by online database GEPIA (Gene Expression Profiling Interactive Analysis, <http://gepia.cancer-pku.cn/>), UALCAN (<http://ualcan.path.uab.edu/analysis.html>), and Prognostic Database (<http://genomics.jefferson.edu/proggene/>). The mRNA expressions of *RANK* in CRC cell lines were analyzed using the CCLE database (<https://portals.broadinstitute.org/ccle/home>). Correlation analysis between gene expression in tissues of CRC patients was computed from cBioPortal (www.cbioportal.org), TIMER (Tumor IMMune Estimation Resource, <https://cistrome.shinyapps.io/timer/>), and GEPIA. CHIP-seq datasets were collected from the ENCODE Project Consortium (<https://www.encodeproject.org/>).

Statistical analysis

Statistical analysis was performed using SPSS 20.0 and GraphPad Prism 6.0. The indicated protein levels to GAPDH are quantified using ImageJ software. Data were compared by Student's *t* test or one-way ANOVA test. The χ^2 test and Fisher's exact test were used to analyze the relationship between RANK expression and clinical characteristics. Survival curves were plotted with the Kaplan–Meier method with the log-rank test. Cox regression was employed for univariate and multivariate analyses. Variables with a *P* value < 0.05 in univariate analysis were included in multivariate analysis. All data are presented as the mean \pm SD. *P* value < 0.05 was considered statistically significant.

Acknowledgements

We thank the members of the Zhu lab for their helpful discussion.

Author details

¹Scientific Research Center, The Seventh Affiliated Hospital, Sun Yat-sen University, Shenzhen, China. ²Department of Pathology, The Seventh Affiliated Hospital, Sun Yat-sen University, Shenzhen, China. ³Division of Hematology/Oncology, Department of Pediatrics, The Seventh Affiliated Hospital, Sun Yat-sen University, Shenzhen, China. ⁴Center of Digestive Diseases, The Seventh Affiliated Hospital, Sun Yat-sen University, Shenzhen, China. ⁵Zhongshan School of Medicine, Sun Yat-sen University, Guangzhou, China. ⁶Department of Orthopaedic Surgery, The Seventh Affiliated Hospital, Sun Yat-sen University, Shenzhen, China

Author contributions

C.M.Z. and L.P.Y. conceived and designed the project, analyzed data, and critically revised the manuscript. Q.L. and Y.W. designed and performed experiments, analyzed data, wrote, and edited the manuscript. Y.S.L., Q.Q.Z., W.L.X., N.N.T., L.F.H., T.L.A., D.Z., and A.Q.Y. performed experiments, analyzed data, and critically revised the manuscript. S.Y.L. designed experiments, provided instructions, and critically revised the manuscript. All the authors read and approved the final paper.

Funding

This work was supported by the funds from the Research Start-up Fund of the Seventh Affiliated Hospital, Sun Yat-sen University (ZSQYBRJH0003), and the National Natural Science Foundation of China (82072905 and 81802666).

Conflict of interest

The authors declare no competing interests.

Ethics statement

This study was approved by the Ethics Committee of Sun Yat-sen University.

Publisher's note

Springer Nature remains neutral with regard to jurisdictional claims in published maps and institutional affiliations.

Supplementary information The online version contains supplementary material available at <https://doi.org/10.1038/s41419-021-03642-7>.

Received: 17 December 2020 Revised: 13 March 2021 Accepted: 15 March 2021

Published online: 01 April 2021

References

- Lacey, D. L. et al. Osteoprotegerin ligand is a cytokine that regulates osteoclast differentiation and activation. *Cell* **93**, 165–176 (1998).

- Rao, S., Cronin, S. J. F., Sigl, V. & Penninger, J. M. RANKL and RANK: from mammalian physiology to cancer treatment. *Trends Cell Biol.* **28**, 213–223 (2018).
- Walsh, M. C. & Choi, Y. Biology of the RANKL–RANK–OPG system in immunity, bone, and beyond. *Front. Immunol.* **5**, 511 (2014).
- Jones, D. H. et al. Regulation of cancer cell migration and bone metastasis by RANKL. *Nature* **440**, 692–696 (2006).
- Luo, J. L. et al. Nuclear cytokine-activated IKK α controls prostate cancer metastasis by repressing Maspin. *Nature* **446**, 690–694 (2007).
- Tan, W. et al. Tumour-infiltrating regulatory T cells stimulate mammary cancer metastasis through RANKL–RANK signalling. *Nature* **470**, 548–553 (2011).
- Sisay, M., Mengistu, G. & Edessa, D. The RANK/RANKL/OPG system in tumorigenesis and metastasis of cancer stem cell: potential targets for anticancer therapy. *Oncotargets Ther.* **10**, 3801–3810 (2017).
- Renema, N., Navet, B., Heymann, M. F., Lezot, F. & Heymann, D. RANK–RANKL signalling in cancer. *Biosci. Rep.* **36**, e00366 (2016).
- Santini, D. et al. Expression pattern of receptor activator of NF κ B (RANK) in a series of primary solid tumors and related bone metastases. *J. Cell. Physiol.* **226**, 780–784 (2011).
- Paget, S. The distribution of secondary growths in cancer of the breast. 1889. *Cancer Metastasis Rev.* **8**, 98–101 (1989).
- Maurizi, A. & Rucci, N. The osteoclast in bone metastasis: player and target. *Cancers* **10**, 218 (2018).
- Cheng, M. L. & Fong, L. Effects of RANKL-targeted therapy in immunity and cancer. *Front. Oncol.* **3**, 329 (2014).
- Palafox, M. et al. RANK induces epithelial–mesenchymal transition and stemness in human mammary epithelial cells and promotes tumorigenesis and metastasis. *Cancer Res.* **72**, 2879–2888 (2012).
- Reynaud, C. et al. Lysyl oxidase is a strong determinant of tumor cell colonization in bone. *Cancer Res.* **77**, 268–278 (2017).
- Wei, Y. et al. Heterologous expression, purification and function of the extracellular domain of human RANK. *BMC Biotechnol.* **17**, 87 (2017).
- Morony, S. et al. The inhibition of RANKL causes greater suppression of bone resorption and hypercalcemia compared with bisphosphonates in two models of humoral hypercalcemia of malignancy. *Endocrinology* **146**, 3235–3243 (2005).
- Tan, W. et al. Tumour-infiltrating regulatory T cells stimulate mammary cancer metastasis through RANKL–RANK signalling. *Nature* **470**, 548–553 (2011).
- Bian, Z. Q. et al. Overexpressed ACP5 has prognostic value in colorectal cancer and promotes cell proliferation and tumorigenesis via FAK/PI3K/AKT signaling pathway. *Am. J. Cancer Res.* **9**, 22–35 (2019).
- Takayanagi, H. et al. Induction and activation of the transcription factor NFATc1 (NFAT2) integrate RANKL signaling in terminal differentiation of osteoclasts. *Dev. Cell* **3**, 889–901 (2002).
- Matsumoto, M. et al. Essential role of p38 mitogen-activated protein kinase in cathepsin K gene expression during osteoclastogenesis through association of NFATc1 and PU.1. *J. Biol. Chem.* **279**, 45969–45979 (2004).
- Crabtree, G. R. Generic signals and specific outcomes: signaling through Ca²⁺, calcineurin, and NF-AT. *Cell* **96**, 611–614 (1999).
- ENCODE Project Consortium. An integrated encyclopedia of DNA elements in the human genome. *Nature* **489**, 57–74 (2012).
- Partington, G. A., Fuller, K., Chambers, T. J. & Pondel, M. Mitf–PU.1 interactions with the tartrate-resistant acid phosphatase gene promoter during osteoclast differentiation. *Bone* **34**, 237–245 (2004).
- Luchin, A. et al. Genetic and physical interactions between Microphthalmia transcription factor and PU.1 are necessary for osteoclast gene expression and differentiation. *J. Biol. Chem.* **276**, 36703–36710 (2001).
- Negishi-Koga, T. & Takayanagi, H. Ca²⁺–NFATc1 signaling is an essential axis of osteoclast differentiation. *Immunol. Rev.* **231**, 241–256 (2009).
- Sobradillo, D. et al. A reciprocal shift in transient receptor potential channel 1 (TRPC1) and stromal interaction molecule 2 (STIM2) contributes to Ca²⁺ remodeling and cancer hallmarks in colorectal carcinoma cells. *J. Biol. Chem.* **289**, 28765–28782 (2014).
- Villalobos, C., Hernández-Morales, M., Gutiérrez, L. G. & Núñez, L. TRPC1 and ORAI1 channels in colon cancer. *Cell Calcium* **81**, 59–66 (2019).
- Jardin, I., Lopez, J. J., Salido, G. M. & Rosado, J. A. Store-operated Ca entry in breast cancer cells: remodeling and functional role. *Int. J. Mol. Sci.* **19**, 4053 (2018).
- Hogan, P. G., Lewis, R. S. & Rao, A. Molecular basis of calcium signaling in lymphocytes: STIM and ORAI. *Annu. Rev. Immunol.* **28**, 491–533 (2010).

30. Zhang, S. L. et al. STIM1 is a Ca^{2+} sensor that activates CRAC channels and migrates from the Ca^{2+} store to the plasma membrane. *Nature* **437**, 902–905 (2005).
31. Zhang, Z. et al. STIM1, a direct target of microRNA-185, promotes tumor metastasis and is associated with poor prognosis in colorectal cancer. *Oncogene* **34**, 4808–4820 (2015).
32. Wang, J. Y. et al. STIM1 overexpression promotes colorectal cancer progression, cell motility and COX-2 expression. *Oncogene* **34**, 4358–4367 (2015).
33. Kuroda, Y., Hisatsune, C., Nakamura, T., Matsuo, K. & Mikoshiba, K. Osteoblasts induce Ca^{2+} oscillation-independent NFATc1 activation during osteoclastogenesis. *Proc. Natl Acad. Sci. USA* **105**, 8643–8648 (2008).
34. Van Cutsem, E., Cervantes, A., Nordlinger, B. & Arnold, D. Metastatic colorectal cancer: ESMO Clinical Practice Guidelines for diagnosis, treatment and follow-up. *Ann. Oncol.* **25**, iii1–iii9 (2014).
35. Tauriello, D. V. F., Calon, A., Lonardo, E. & Batlle, E. Determinants of metastatic competency in colorectal cancer. *Mol. Oncol.* **11**, 97–119 (2017).
36. Beristain, A. G., Narala, S. R., Di Grappa, M. A. & Khokha, R. Homotypic RANK signaling differentially regulates proliferation, motility and cell survival in osteosarcoma and mammary epithelial cells. *J. Cell Sci.* **125**, 943–955 (2012).
37. Kupas, V. et al. RANK is expressed in metastatic melanoma and highly upregulated on melanoma-initiating cells. *J. Invest. Dermatol.* **131**, 944–955 (2011).
38. Tripathi, M. K. et al. Nuclear factor of activated T-cell activity is associated with metastatic capacity in colon cancer. *Cancer Res.* **74**, 6947–6957 (2014).
39. Wang, G. et al. The critical role of calcineurin/NFAT (C/N) pathways and effective antitumor prospect for colorectal cancers. *J. Cell. Biochem.* **120**, 19254–19273 (2019).
40. Oddie, G. W. et al. Structure, function, and regulation of tartrate-resistant acid phosphatase. *Bone* **27**, 575–584 (2000).
41. Chao, T. Y., Wu, Y. Y. & Janckila, A. J. Tartrate-resistant acid phosphatase isoform 5b (TRACP 5b) as a serum maker for cancer with bone metastasis. *Clin. Chim. Acta* **411**, 1553–1564 (2010).
42. Burgess, T. L. et al. The ligand for osteoprotegerin (OPGL) directly activates mature osteoclasts. *J. Cell Biol.* **145**, 527–538 (1999).
43. Honig, A. et al. Increased tartrate-resistant acid phosphatase (TRAP) expression in malignant breast, ovarian and melanoma tissue: an investigational study. *BMC Cancer* **6**, 199 (2006).
44. Zenger, S. et al. Differential expression of tartrate-resistant acid phosphatase isoforms 5a and 5b by tumor and stromal cells in human metastatic bone disease. *Clin. Exp. Metastasis* **28**, 65–73 (2011).
45. Scott, K. L. et al. Proinvasion metastasis drivers in early-stage melanoma are oncogenes. *Cancer Cell* **20**, 92–103 (2011).
46. Wu, L. et al. FUN14 domain-containing 1 promotes breast cancer proliferation and migration by activating calcium-NFATc1-BMI1 axis. *EBioMedicine* **41**, 384–394 (2019).
47. Jiang, Y. et al. Transcription factor NFAT5 contributes to the glycolytic phenotype rewiring and pancreatic cancer progression via transcription of PGK1. *Cell Death Dis.* **10**, 948 (2019).